Available online at www.eccomasproceedia.org
Eccomas Proceedia SMART (2023) 1611-1622

ECCOMAS
Proceedia

X ECCOMAS Thematic Conference on Smart Structures and Materials
SMART 2023
D.A. Saravanos, A. Benjeddou, N. Chrysochoidis and T. Theodosiou (Eds)

MODELING AND SIMULATION OF DEFORMATION AND CAPACITANCE OF A SUBSTITUE SYSTEM OF A SENSOR-INTEGRATED JAW COUPLING

Johannes D. M. Menning[1], Artem Prokopchuk[2], Arthur Ewert[3], Berthold Schlecht[3], E.-F. Markus Henke[2], and Thomas Wallmersperger[1]

[1]Institute of Solid Mechanics, Technische Universität Dresden, George-Bähr-Str. 3c, 01069 Dresden
e-mail: johannes.menning@tu-dresden.de

[2]Institute for Semiconductors and Microsystems, Technische Universität Dresden, Nöthnitzer Straße 64, 01069 Dresden

[3]Institute of Machine Elements and Machine Design, Technische Universität Dresden, Münchner Platz 3, 01069 Dresden

Abstract. In today's world, the desire for things to be "smart" has also reached machine elements. In the current work, we investigate a substitute system for a sensor-integrated jaw coupling in which a dielectric elastomer sensor (DES) is integrated into the teeth of the elastic gear rim. Compression of the teeth during loading causes the sensor to deform, resulting in an increase in capacitance of the DES. The aim of the present work is to model the relationship between the capacity of the sensor and the compressive force which acts on the substitue system. For this purpose, a finite element (FE) analysis of the substitue system consisting of the DES, the gear rim material and two strain amplifiers is carried out. The resulting change of the capacity due to the mechanical loading is determined both analytically and numerically. Finally, the computed capacities are compared to experimental data.

Key words: Sensor-integrating machine elements, Dielectric elastomers, Modeling, Simulation

1 Introduction

Today, components and machines are supposed to be "smart". In order to realize a smart machine, we need information about the parts that make up the machine, i.e. the machine elements such as couplings. A subgroup of these couplings are elastic couplings which are used to transmit torque between two rotation shafts and to compensate for misalignment. Menning et al. [1] presented a numerical model for the simulation of jaw couplings. During the operation of a machine it is desirable to have information about the transmitted torque to e.g. inspect the machine after load peaks or to monitor the process and regulate the torque to keep it at a desirable level. One method to measure this torque is to insert dielectric elastomer sensors (DES) into the

Peer-review under responsibility of the organizing committee of SMART 2023.
doi: 10.7712/150123.9933.443570

teeth of the gear rim of the jaw coupling. During use, the teeth of the gear rim will deform and so does the elastomer sensor. Dielectric elastomer sensors consist out of an elastomer which is located between two compliant electrodes. It follows that they can be modeled electrically as plate capacitors, with the elastomer serving as the dielectric. If a mechanical stress is applied on the dielectric elastomer, it will deform. This results in a change of its height, which in turn leads to an increase of the capacitance [2, 3]. This change can then be evaluated in order to get information about the applied force or torque when used in the jaw coupling. The aim of the current work is to present a combination of a numerical and an analytical model of the sensor and a substitute model of its implementation in the jaw coupling to predict the mechanical and electrical behavior of such a sensor. For this purpose, the general structure of the investigated sensor is described in section 2. The subsequent simulation is divided into two parts. In the first part (I) the deformation of the DES due to a mechanical load is simulated via the finite element method. The finite element tool ABAQUS is used to solve the mechanical field. The mechanical model with the used material models is described in section 3. In the second part (II) the change in capacitance due to the deformation of the DES is evaluated. This is described in section 4. In the current work, the displacement-based controlled finite element method is employed. It follows, that the change of the thicknesses of the capacitive layers of the sensor could also accurately be determined without the use of an elaborate model. For this, the total displacement of the sensor would be equally distributed to all layers of the sensor, if the stiffness were the same for all layers. Subsequently, the capacity can be determined on the basis of the new heights. However, please note that the model presented here is used as a first approach to test different configurations of DES, which are later used as sensors in a jaw coupling. In such a coupling the displacements are not known a priori for different load cases, shaft displacements and temperatures. Additionally, the aim of the sensor and therefore of the presented model of the sensor is to give a relationship between the capacitance and the applied force respectively the applied torque. This is only possible in conjunction with a numerical model, such as the one described in this paper. The obtained results with this model are shown in section 6. Finally, in section 7 a conclusion is drawn and an outlook is given.

2 Modeling of dielectric elastomer sensor and substitute system

In Prokopchuk et al. [4] the manufacturing of a new dielectric elastomer sensor is described. This sensor is made up of alternating dielectric, and electrode layers which are placed upon an Elastosil base. SilGel [5] is used to glue the single layers together. In the following, the material for the dielectric layer is Elastosil if not stated otherwise. The electrode layers are made up of conductive ink based on Ecoflex-20 and carbon black. They have a circular shape with a diameter of $d_{\text{electrode}}$ and two pins at each end to connect the electrodes to a power source. The dielectric layer has a similar, but slightly larger shape. In the current work, the diameters of $d_{\text{electrode}}$ and $d_{\text{dielectric}}$ are set to $d_{\text{electrode}} = 3\,\text{mm}$ and $d_{\text{dielectric}} = 4\,\text{mm}$, respectively a schematic representation of this configuration can be seen in Figure 1. As can be seen, the total height of each capacitive layer consists of the actual dielectric layer and the part of the glue layer which is above the respective electrode, $h_{\text{capa glue-layer}} = h_{\text{glue-layer}} - h_{\text{electrode-layer}}$. Due to the stacked

configuration, the DES can be considered as several capacitors connected in parallel where the capacity of the single capacitors adds up to the total capacity. The total capacity of the DES can be increased, for example, by increasing the number of capacitive layers.

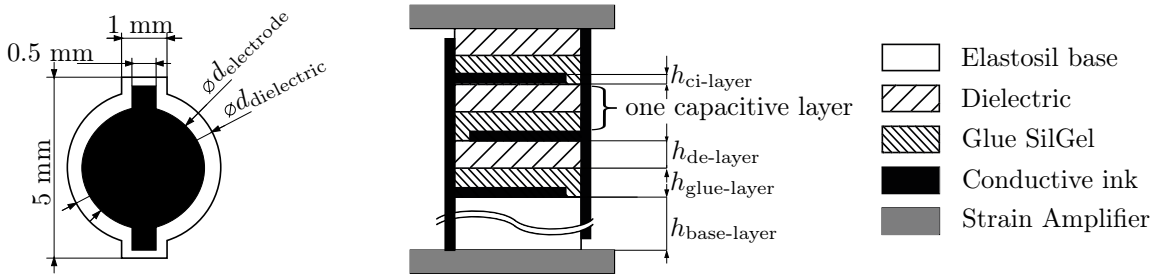

Figure 1: Schematic representation of the structure of the dielectric elastomer sensor.

The gear rim of a jaw coupling is typically made of thermoplastic polyurethane (TPU). In the present research, not an entire tooth is modeled but a hollow cylinder in order to reduce the complexity. Please note that in Figure 1 this hollow cylinder has been omitted for the sake of clarity. The teeth, and therefore also the cylinder for the substitute model, will have a greater height than the sensor. To ensure that the sensor is experiencing the same amount of displacement as the teeth/cylinder, the upper and lower ends have strain amplifiers attached to them. These strain amplifiers are made of steel and are therefore much stiffer than the sensor, which is why all the deformation is passed on to the sensor.

3 Mechanical model

Some of the used materials like (i) carbon black, for the electrodes, (ii) SilGel for the glue, or (iii) TPU of which the gear rim is made up, exhibit viscoelastic material behavior. During the use of a jaw coupling, the teeth of the gear rim compress substantially. It follows, that the dielectric elastomer sensor will exhibit large deformations as well. In order to model this behavior, a hyperviscoelastic material model is used for both the sensor and the TPU to account for the combination of large deformation and viscoelastic material behavior. In the following, we will give a short introduction into the used equations to model this behavior. A more detailed overview of the modeling of hyperviscoelastic materials can be e.g. found in [6, 7].

One possibility to represent a viscoelastic material is by a single spring which is in parallel to a series of N spring-dashpot pairs, where the latter ones represent the viscoelastic material behavior. A typical approach to model such a material is the multiplicative decomposition of the deformation gradient $\boldsymbol{F} = \mathbf{1} + \nabla \boldsymbol{u}$ with $\boldsymbol{u}$ being the displacement, into an elastic and a viscous part [6]

$$\boldsymbol{F} = \boldsymbol{F}^e \cdot \boldsymbol{F}^v \,. \tag{1}$$

It can be shown that by complying to the first and second law of thermodynamics, the Kirchhoff stress $\boldsymbol{\tau}$ is a function of the free energy Ψ. In ABAQUS [8], $\boldsymbol{\tau}$ is derived by an ansatz for Ψ with a single set of material parameters

$$\boldsymbol{\tau} = \sum_{i=0}^{N} s_i \left(\boldsymbol{F}_i^e \cdot 2 \frac{\partial \Psi}{\partial \boldsymbol{C}_i^e} \cdot (\boldsymbol{F}_i^e)^T \right) , \tag{2}$$

where $\boldsymbol{C}_i^e$ are the elastic right Cauchy-Green tensors of the single spring and spring-dashpot pairs and s_i are scaling factors [8]. Please note that $\sum_{i=0}^{N} s_i = 1$ holds. In the current work, the quasi static mechanical behavior of the substitute model is investigated by neglecting the external body forces. This simplifies the balance of linear momentum to

$$\mathbf{0} = J \nabla \cdot \left(\frac{\boldsymbol{\tau}}{J} \right) , \tag{3}$$

with $J = \det(\boldsymbol{F})$ being the determinant of the deformation gradient, which is a measure of the change in volume. For the viscoelastic material, an evolution equation for the internal variable $\boldsymbol{C}^v$

$$\dot{\boldsymbol{C}}^v = 2(\boldsymbol{F}^v)^{\mathrm{T}} \cdot \dot{\bar{\gamma}} \boldsymbol{N} \cdot \boldsymbol{F}^v \tag{4}$$

has to be solved additionally to equation (3), cf. [9], with $\dot{\bar{\gamma}}$ being the equivalent creep strain rate and $\boldsymbol{N} = \frac{\boldsymbol{\tau}_{\mathrm{iso}}^v}{||\boldsymbol{\tau}_{\mathrm{iso}}^v||}$.

Material model As a first assumption, in the absence of more precise data, the elastomer components of the sensor are assumed to be incompressible. The same assumption was made for the TPU, whose incompressibility was described by Qi and Boyce [10]. In order to model this behavior, the free energy is split into an isochoric and a volumetric part. A free energy of the type proposed by Yeoh [11] and a volumetric term, as it is used in ABAQUS, were used as the hyperelastic material model

$$\Psi = c_1(\bar{I}_1 - 3) + c_2(\bar{I}_1 - 3)^2 + c_3(\bar{I}_1 - 3)^3 + \frac{K_0}{2}(J-1)^2 , \tag{5}$$

with $\bar{I}_1 = J^{-\frac{2}{3}} \boldsymbol{C}$, K_0 being the bulk modulus and c_1, c_2, c_3 being material parameters.

For the evolution equation of the internal variable a simplified version of the power law approach as it is used in ABAQUS was employed [8]

$$\dot{\bar{\gamma}}^v = \left(\frac{q}{q_0} \right)^n , \tag{6}$$

with n and q_0 being material parameters and q the effective deviatoric Kirchhoff stress.

4 Electrical model

In order to model the change in capacitance due to the deformation of the DES two different variants were compared with each other.

4.1 Analytical determination of the capacity

In the first variant the current heights of the capacitive layers, determined via the current z-coordinate for each time step, are inserted in the equation for a parallel plate capacitor consisting out of i layers

$$C = \frac{A}{\sum_i \frac{h_i}{\varepsilon_i}} \tag{7}$$

with C being the capacity, ε_0 the permittivity of vacuum, ε_r the relative permittivity of the material, $\varepsilon_i = \varepsilon_0 \cdot (\varepsilon_r)_i$ the permittivity of the respective material, A the area of the electrodes and h_i the heights of the dielectric layer and the glue layer which form the capacitive layer. The conductive ink, which forms the electrode layer is, among others, based on Ecoflex 00-20. In the current paper the electrode layer is assumed to be incompressible. It follows that when the height h changes, the area also changes which further increases the resulting capacity. This change in area can be determined by converting the formula for calculating the initial volume V_0, with the initial diameter d_0 and the initial height h_0 according to the diameter

$$V_0 = \frac{\pi}{4}\, d_0^2\, h_0\,; \quad d_{\text{new}} = \sqrt{\frac{4\, V_0}{\pi\, h}}\,, \tag{8}$$

which can then be used to calculate the new area $A_{\text{new}} = \frac{\pi}{4}\, d_{\text{new}}^2$.

4.2 Numerical determination of the capacity

In the second variant the capacity is determined numerically via the finite element tool FEniCSx [12]. For this purpose the ABAQUS mesh (.inp) is updated with the current coordinates of the deformed mesh (ABAQUS output: COORD) for each point in time. The updated input file is then converted to xdmf-format so that it can be read by FEniCSx. Based on these deformed meshes an electrostatic simulation is performed. In the following the electrostatic model and the determination of the capacity will be described. Please note that there is a one-way coupling between the mechanical and the electric field, i.e. the mechanical deformation influences the electric field, but not vice versa. It follows, that no distinction between reference and current configuration is necessary for the description of the Maxwell equations and the used material equations. Additionally, we consider the dielectric to be ideal, i.e. the relative permittivity ε_r of the dielectric is not a function of the deformation, as described e.g. by [13, 14].

The Maxwell equations for the current configuration are defined as

$$\nabla \times \underline{e} = 0 \tag{9}$$

$$\nabla \cdot \underline{d} = \rho_f \tag{10}$$

with $\underline{e}$ being the electrical field, $\underline{d}$ the dielectric displacement and ρ_f the free charges per unit volume, cf. [15, 16]. Equation (9) can be fulfilled a priori with the introduction of a scalar electric potential ϕ, $\underline{e} = -\nabla\,\phi$. The polarization of a material $\underline{p}$ due to an electrical field $\underline{e}$ is given by [16]

$$\underline{p} = \underline{d} - \varepsilon_0\,\underline{e}\,. \tag{11}$$

For a linear, homogeneous, isotropic dielectric material $\underline{p}$ can be given as [15]

$$\underline{p} = \varepsilon_0(\varepsilon_r - 1)\,\underline{e}\,. \tag{12}$$

Inserting equation (12) into equation (11) yields

$$\underline{d} = \varepsilon_0\varepsilon_r\,\underline{e}\,. \tag{13}$$

For a linear, homogeneous, isotropic dielectric material the electrical free energy Ψ_{el} can be defined as

$$\Psi_{\text{el}} = \frac{1}{2}\,\varepsilon\,\underline{e}\cdot\underline{e}\,. \tag{14}$$

No free charges are present in the dielectric elastomer sensor, i.e. $\rho_f = 0$. Inserting equation (13) into equation (10) and setting $\rho_f = 0$ yields

$$\nabla^2\phi = 0\,. \tag{15}$$

The weak form of equation (15)

$$\int_\Omega -\nabla\phi\cdot\nabla\delta\phi\,\mathrm{d}V + \int_{\partial\Omega}\sigma\,\delta\phi\,\mathrm{d}A = 0 \tag{16}$$

with the scalar weighting function $\delta\phi$, the electrical surface charge σ, volume V and area A was implemented into FEniCSx. The boundary conditions used are described in section 5.

After solving equation (16), the electrical energy can be computed for the whole domain of the capacitive layer

$$W_{\text{electric}} = \int_\Omega \frac{1}{2}\,\varepsilon\,\underline{e}\cdot\underline{e}\,\mathrm{d}V\,. \tag{17}$$

The internal electrical energy for a plate capacitor is given by [17]

$$W_{\text{capacitor}} = \frac{1}{2}\,C\,U^2\,, \tag{18}$$

with U being the electric potential (resp. the potential difference) applied at the electrodes. Please note that equation (18) assumes a homogeneous electric field inside the capacitor. By equating equation (17) and equation (18), i.e. $\int_\Omega \frac{1}{2}\,\varepsilon\,\underline{e}\cdot\underline{e}\,\mathrm{d}V = \frac{1}{2}\,CU^2$ and the knowledge of the applied potential difference, the capacity of the capacitor can be determined.

5 Numerical realization

The used mechanical boundary conditions (BCs) to model the behavior of the substitute system of the sensor-integrated jaw coupling are given in Table 1. To save computational costs only a quarter of the system was modeled. A displacement in z-direction is applied on the top surface to simulate the deformation of the tooth of the gear rim. At the bottom surface the displacement in z-direction is blocked. To account for the employed symmetry, the x-displacement is blocked on the surface **D**, which consists of the combined surfaces of the DES, the TPU and the strain amplifiers in this plane. The same is done for the y-displacement of the nodes on surface **C**. The surfaces on which the BCs are employed are given in Figure 2. For the numerical computation of the capacitance, an electric potential of $\phi = 1\,\mathrm{V}$ or $\phi = -1\,\mathrm{V}$ is applied to the electrode layers.

Table 1: Applied boundary conditions for the finite element model of the substitute system of the jaw coupling.

boundary condition	location
$U_z = -0.1\,\mathrm{mm}$	surface **A**
$U_z = 0$	surface **B**
$U_y = 0$ (y-Symmetry)	surface **C**
$U_x = 0$ (x-Symmetry)	surface **D**

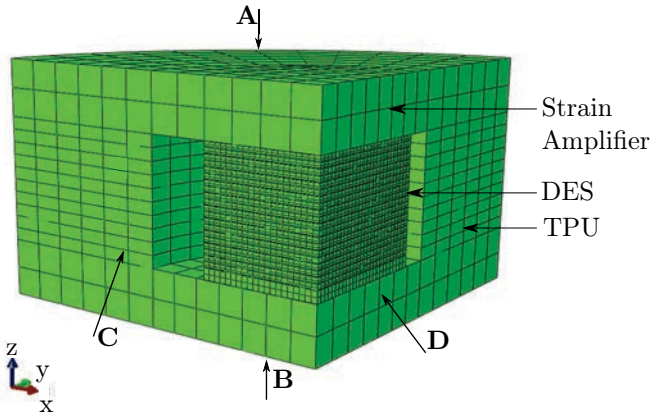

Figure 2: Finite element mesh for a quarter of a DES with 20 capacitive layers with labeled surfaces for the mechanical boundary conditions.

Material parameters Please note that carbon black and SilGel are assumed to have the same material parameters as Ecoflex, for which uniaxial loading-unloading tests were conducted.

Carbon black is mainly made up of Ecoflex. Please note that both materials are much softer than the TPU to have an influence on the resulting force. Only hyperelastic parameters were given for Elastosil [18]. The used material parameters for the mechanical resp. the electrical model are given in Tables 2 and 3.

Table 2: Parameters for the Yeoh free energy (equation (5)) and the power law model (equation (6)) with one Maxwell element. The parameters for the TPU and for Ecoflex were determined via uniaxial loading-unloading tests. The parameters of Elastosil are taken from [18].

Material	c_1 [MPa]	c_2 [MPa]	c_3 [MPa]	K_0 [MPa]	s_{NEQ} [-]	q_0 [MPa]	n [-]
TPU	13.02	-5.16	6.15	2604	0.65	3.37	3.94
Ecoflex-30 0.4	0.062	0.011	2.74E-06	125	0.61	0.01	5.59
Elastosil	0.18	-5.19E-06	2.4E-03	-	-	-	-

Table 3: Relative permittivities ε_r for the different types of silicone used in the DES

Material	ε_r	Reference
Ecoflex-30 0.4 wt% carbon black	2.95	[4]
Elastosil	2.8	[19]
SilGel 612	2.7	[5]

6 Results

In the following, experimental data are compared to the numerical results. Afterwards different configurations of the sensor were investigated, i.e. (i) the number of dielectric layers and (ii) the material for the dielectric layer are varied. The resulting relationships between the force and the analytically and numerically determined capacities are given below. For the following calculations the diameter of the electrodes was set to $d_{\text{electrode}} = 3.0\,\text{mm}$.

6.1 Comparison of numerical and experimental data

For the experiments a sensor with four electrodes, $h_{\text{de-layer}} = 0.035\,\text{mm}$, $h_{\text{capa glue-layer}} = 0.016\,\text{mm}$ and $h_{\text{base-layer}} = 0.1\,\text{mm}$ was used. Additionally, two of these sensors were stacked upon each other to increase the resulting capacity. The two specimen were subjected to a uniaxial loading-unloading test by a tensile testing machine from ZwickRoell. The capacitance of the two sensors were measured using an IM3523 LCR meter from HIOKI, which was connected to the contacts of the sensors using double-ended tester cables with crocodile clips. Two finite element models with the dimensions of the two sensors were used to compare the computational determined values with the experimental data. Two calculations were performed, (i) with and (ii) without the consideration of the change in the area of the electrodes, cf. equation (8). As

can be seen in Figure 3, contradictory to the initial assumption of the change in the area, the agreement between the calculated and experimental capacities is good if the change in area is neglected. Additionally, a small hysteresis can be seen for the experimental data.

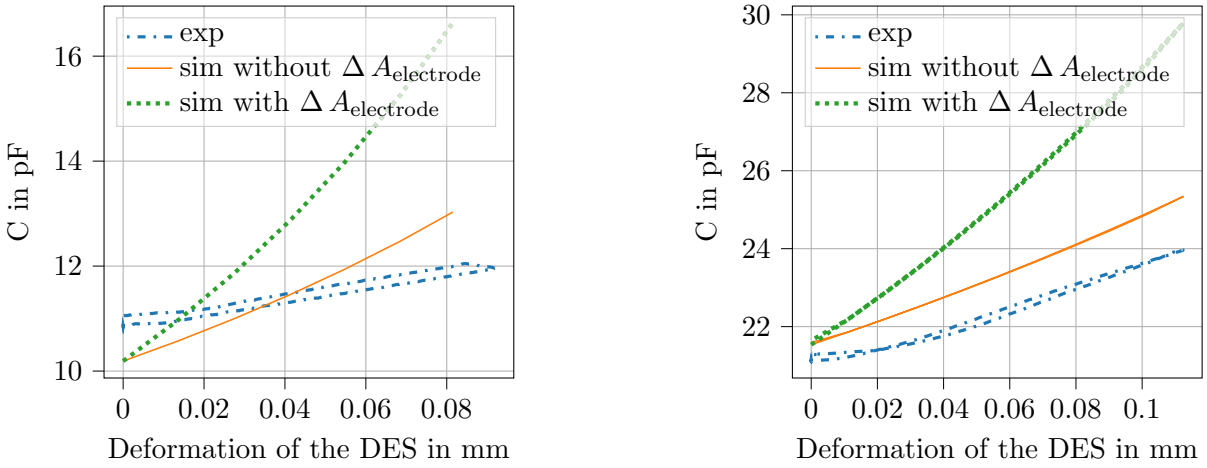

(a) Single DES with 4 electrodes

(b) Two DES stacked upon each other

Figure 3: Comparison of experimentally and computationally determined relationship of capacity and deformation of a single 4ML-DES and two 4ML-DES, which were stacked together.

6.2 Modification of the dielectric material

Finally, the influence of the material for the dielectric layer was investigated. Figure 4 shows the capacitance versus the force for Elastosil and Ecoflex with 0.4% carbon black as material for the dielectric layer. Please note that here the change in area of the electrode is neglected. Due to the higher relative permittivity of Ecoflex compared to Elastosil, cf. Table 3, the resulting capacitance is higher if Ecoflex is used as dielectric material.

6.3 Comparison of analytically and numerically determined capacitances

Figure 5 shows the results for the analytical and numerical determined capacities for four sensor configurations with different numbers of electrodes. The minimal capacity C_{min} represents the capacity before the application of a load and the maximal capacity C_{max} represents the capacity when the sensors are subjected to the maximum applied deformation, which in the current work was set to $\Delta u = 0.1\,\text{mm}$. As expected, the numerically determined capacities are higher than the analytical ones due to the fact, that the former ones also account for the fringe fields at the ends of the electrodes. It can also be observed that the relationship between the number of electrode layers is linear in the analytical model, while it is slightly non-linear in the numerical model. For the analytically determined capacities, the area change of the electrodes was also modeled. The numerical model intrinsically considers the change in area of the electrodes, which in Figure 3 was shown to lead to unrealistic results.

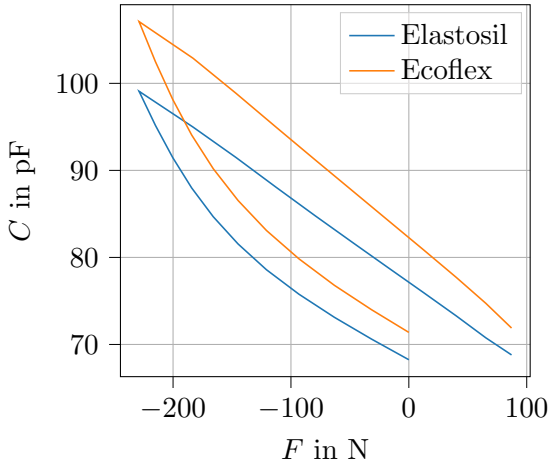

Figure 4: Analytically determined capacity versus force for a DES consisting of 10 capacitive layers with $h_{\text{de-layer}} = 0.02\,\text{mm}$, $h_{\text{capa glue-layer}} = 0.003\,\text{mm}$, subjected to a displacement of $\Delta u = 0.1\,\text{mm}$.

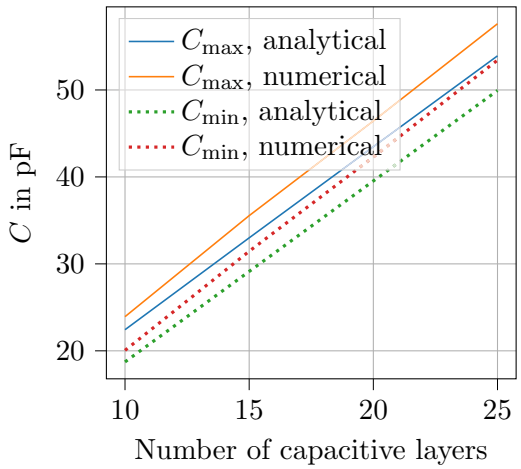

Figure 5: Minimal and maximal values for the analytically (analytical) and numerically (numerical) determined capacity C after the sensor structure which consists out of different numbers of capacitive layers, was subjected to a displacement of $\Delta u = 0.1\,\text{mm}$. The height of the dielectric layers was $h_{\text{de-layer}} = 0.05\,\text{mm}$.

7 Conclusion and outlook

In this paper a computational model for a dielectric elastomer sensor was presented. The model consists of a mechanical model, with which the deformation of the sensor and the resulting force can be determined. The change in capacitance, resulting from the deformation of the sensor, was afterwards determined both analytically and numerically. As expected, the numerical determined capacities were higher than the analytical ones. Additionally the results

from the model were compared to experimental data. It has been shown, that the difference between computed and experimental capacities are much smaller, if the area of the electrodes are assumed to be constant during the deformation. The next step is to incorporated the presented model of the DES into a finite element model of a jaw coupling and validate the resulting torque-capacitance data with experimental data.

Acknowledgement

The support of the German Science Foundation (DFG) within the grants WA 2323/21-1, HE 7385/3-1, SCHL 1736/8-1 (project number: 441853410 and 466661922) is gratefully acknowledged.

REFERENCES

[1] J. Menning, A. Ewert, A. Prokopchuk, B. Schlecht, M. Henke, and T. Wallmersperger, "Finite element based modeling and simulation of an elastomer gear rim," *accepted in PAMM*, 2023.

[2] S. Rosset and H. R. Shea, "Small, fast, and tough: Shrinking down integrated elastomer transducers," *Applied Physics Reviews*, vol. 3, no. 3, p. 031105, 2016.

[3] M. Franke, A. Ehrenhofer, S. Lahiri, E.-F. Henke, T. Wallmersperger, and A. Richter, "Dielectric elastomer actuator driven soft robotic structures with bioinspired skeletal and muscular reinforcement," *Frontiers in Robotics and AI*, vol. 7, p. 510757, 2020.

[4] A. Prokopchuk, A. Ewert, J. Menning, A. Richter, B. Schlecht, T. Wallmersperger, and E.-F. M. Henke, "Manufacturing of soft capacitive strain sensor based on dielectric elastomeric material for an elastic element of a jaw coupling," *submitted to Smart Materials and Structures*, 2023.

[5] "Properties of Wacker SilGel 612," https://www.wacker.com/h/en-us/silicone-rubber/silicone-gels/wacker-silgel-612-ab/p/000007546, retrieved at 11.12.2022, 2022.

[6] S. Reese and S. Govindjee, "Theoretical and numerical aspects in the thermo-viscoelastic material behaviour of rubber-like polymers," *Mechanics of Time-Dependent Materials*, vol. 1, pp. 357–396, 1997.

[7] J. S. Bergström and M. Boyce, "Constitutive modeling of the large strain time-dependent behavior of elastomers," *Journal of the Mechanics and Physics of Solids*, vol. 46, no. 5, pp. 931–954, 1998.

[8] I. Lapczyk and J. A. Hurtado, "A viscoelastic-elastoplastic finite strain framework for modeling polymers," in *ASME International Mechanical Engineering Congress and Exposition*, vol. 46583. American Society of Mechanical Engineers, 2014, p. V009T12A096.

[9] P. Areias and K. Matouš, "Finite element formulation for modeling nonlinear viscoelastic elastomers," *Computer Methods in Applied Mechanics and Engineering*, vol. 197, no. 51-52, pp. 4702–4717, 2008.

[10] H. J. Qi and M. C. Boyce, "Stress–strain behavior of thermoplastic polyurethanes," *Mechanics of materials*, vol. 37, no. 8, pp. 817–839, 2005.

[11] O. H. Yeoh, "Some forms of the strain energy function for rubber," *Rubber Chemistry and technology*, vol. 66, no. 5, pp. 754–771, 1993.

[12] M. W. Scroggs, I. A. Baratta, C. N. Richardson, and G. N. Wells, "Basix: a runtime finite element basis evaluation library," *Journal of Open Source Software*, vol. 7, no. 73, p. 3982, 2022.

[13] A. Ask, A. Menzel, and M. Ristinmaa, "Modelling of viscoelastic dielectric elastomers with deformation dependent electric properties," *Procedia Iutam*, vol. 12, pp. 134–144, 2015.

[14] M. Mehnert, M. Hossain, and P. Steinmann, "Experimental and numerical investigations of the electro-viscoelastic behavior of vhb 4905tm," *European Journal of Mechanics-A/Solids*, vol. 77, p. 103797, 2019.

[15] A. Büschel, S. Klinkel, and W. Wagner, "Dielectric elastomers–numerical modeling of nonlinear visco-electroelasticity," *International Journal for Numerical Methods in Engineering*, vol. 93, no. 8, pp. 834–856, 2013.

[16] L. Dorfmann and R. W. Ogden, "Nonlinear electroelasticity: material properties, continuum theory and applications," *Proceedings of the Royal Society A: Mathematical, Physical and Engineering Sciences*, vol. 473, no. 2204, p. 20170311, 2017.

[17] C. Jean-Mistral, S. Iglesias, S. Pruvost, J. Duchet-Rumeau, and S. Chesné, "Dielectric elastomer for stretchable sensors: Influence of the design and material properties," in *Electroactive Polymer Actuators and Devices (EAPAD) 2016*, vol. 9798. SPIE, 2016, pp. 479–488.

[18] D. Utkan, D. Maruthavanan, A. Schimanowski, and A. Seibel, "Compression behavior of typical silicone rubbers for soft robotics applications at elevated temperatures," in *2021 IEEE 4th International Conference on Soft Robotics (RoboSoft)*. IEEE, 2021, pp. 539–542.

[19] "ELASTOSIL Film Ultrathin Silicone Film for High-Precision Solutions," https://www.wacker.com/h/de-de/medias/7091-EN.pdf, retrieved at 28.11.2022, 2022.